This review discusses theoretical and practical developments concerning the He^3–He^4 dilution refrigerator. Properties of He^3–He^4 solutions are briefly discussed in terms of the weakly interacting Fermi-Dirac gas model and re-used to calculate the behaviour of dilution refrigerators. The thermodynamic behaviour of the dilution process is first discussed, and then an analysis of various types of heat exchangers is presented. The use of nearly optimum heat exchangers, designed by the method outlined here, can significantly reduce the liquid volumes required and/or reduce the low temperature limit of the continuous dilution refrigerator. With smaller liquid volumes, the refrigerator can be cooled down and can reach thermal equilibrium more rapidly. Discussions of various practical considerations and recent developments in hardware are also included. Some suggestions for future work and speculations on trends are presented.

Dilution refrigerator technology

R. Radebaugh and J. D. Siegwarth

The development of the He^3–He^4 dilution refrigerator has advanced so rapidly in the last five years that a review of the work at this time could be helpful to those who are designing or using such a device. In addition, some new ideas and concepts are presented. Advances, particularly in the area of heat exchangers, are still occurring at such a pace that this review could soon be outdated, at least as far as practical developments in heat exchangers are concerned.

The theory of the He^3–He^4 dilution process has played a significant role in the evolvement of present day dilution refrigerators, particularly if one recalls that H. London's original proposal [1] for the process in 1951 was based on the theory [2] of Fermi liquids and preceded by thirteen years the first refrigerator of Das et al.[3] London's second proposal,[4] which utilized the discovery [5] a few years earlier of phase separation in He^3–He^4 solutions, was very explicit regarding the scheme for carrying out the continuous dilution process and led directly to the first refrigerator of Das et al, two years later. However, at the time of the first really successful refrigerators,[6,7] the theory was limited to mostly qualitative ideas, and the few quantitative predictions had not taken into account degenerate effects which occur in the dilute He^3 solutions below a few tenths K. The theoretical limitations of the refrigerator were not known. Prodded by the sudden interest in the refrigerators, the theory of the device as well as practical improvements advanced rapidly after 1966. Several publications on the theory have appeared recently where degenerate effects in the solutions are taken into account. The first of these [8–10] neglected He^3–He^3 interactions, whereas later papers [11–14] took these weak interactions into account and appear to give quite accurate results for the thermodynamic behaviour of the refrigerators. The concepts in these later papers are discussed in some detail here. Theoretical advances beyond this point are now taking place on heat exchanger behaviour and are, for the most part, more for design information than for a basic understanding of the refrigeration cycle. However, some rather interesting results have come from the heat exchanger analyses. A very thorough description of practical considerations for reaching continuous temperatures of 0·010 K was presented by Wheatley et al,[13] in 1968. Considerable progress has been made since that time, and many of these new ideas are discussed. Since the completion of this work, Wheatley and co-workers have published [63] an extension to their earlier work.[13] They present much new information on co-axial heat exchangers which should be very useful, and point out a puzzling problem in trying to reach temperatures below 0·010 K.

The authors are with the Cryogenics Division, NBS Institute for Basic Standards, Boulder, Colorado 80302, USA. Received 3 April 1971.

Properties of He^3–He^4 solutions

A description of the refrigerator naturally depends on the properties of the working fluid, so first we shall consider some of these properties. Figure 1 is the phase diagram of He^3–He^4 solutions and shows that phase separation takes place below about 0·86 K, as first seen by Walters and Fairbanks.[5] If a mixture of He^3 and He^4 containing a molar fraction X of He^3 is cooled below the phase separation line, the solution separates into two phases. The concentrated phase (concentration X_μ) floats on top of the dilute phase (concentration X_l). The two phases are in equilibrium with each other, just as in the case of a liquid and its vapour. Thus the He^3 chemical potential, μ_3, must be equal in both phases. The He^4 in the dilute phase is superfluid below the λ line, whereas in the concentrated phase it is not. In the dilute phase, then, the relation

$$\nabla \mu_4 = 0 \qquad (1)$$

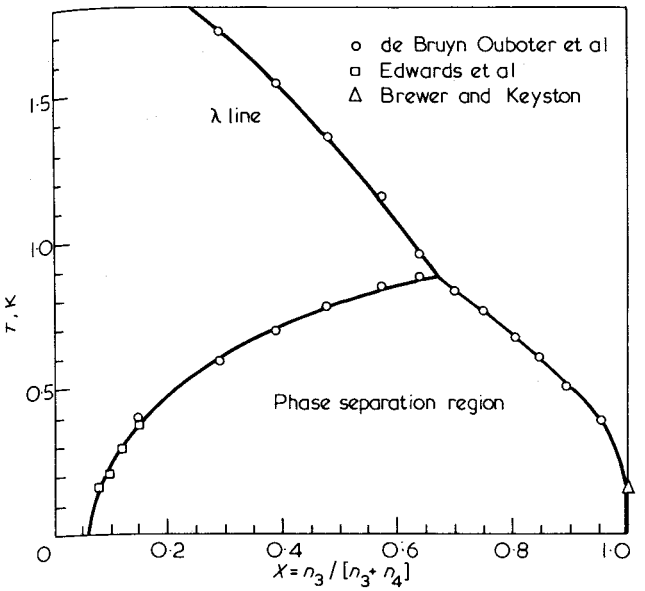

Figure 1. Phase diagram of He^3–He^4 solutions. The data points are from several authors,[15–17] and the detailed behaviour at the intersection of the λ and phase separation lines is from the work of Graf et al [18]

must hold [12] in equilibrium, where μ_4 is the He^4 chemical potential in solution. In addition to the data points shown in Figure 1, there are very extensive measurements of the dilute phase separation line by Ifft et al,[19] using dielectric measurements and later by Schermer et al,[20] using neutron transmission. Unfortunately the two results are not in perfect agreement. The limiting solubility, X_0, of He^3 in He^4 at 0 K is 0·0640 ± 0·0007 from the former and 0·0684 ± 0·0006 from the latter. Recently other dielectric measurements [21] and osmotic-pressure measurements [22] give a value of 0·0660 ± 0·0006 for X_0. Accurate numerical results for the behaviour of the refrigerator rely on a measured value for X_0. All the results reported here are based on the figure 0·0640, simply because only that figure was available when the calculations [11] were made. A different value for X_0 would alter primarily the heat absorption rate of the refrigerator and will be discussed later.

It is apparent from the phase diagram that at temperatures applicable to the dilution refrigerator, dilute He^3 solutions and nearly pure He^3 are the only solutions possible. Properties of pure He^3 necessary for describing the refrigerator have all been measured quite accurately to temperatures as low as a few millikelvin. However little is known about the properties of concentrated solutions below 0·4 K, that is, solutions in the range 80–95% He^3, but reasonable estimates can be made. These are the concentrations usually circulated in actual refrigerators, and the specific heat just below the phase separation temperature can be considerably higher than for pure He^3. This places an uncertainty in the behaviour of the higher temperature part of the refrigerator such as the upper heat exchangers. Several measurements have been made on various properties of dilute He^3 solutions but, because of the added dimensions of concentration, insufficient data exist to completely map, from the data alone, the properties as a function of both temperature and concentration. Fortunately a rather simple and accurate theoretical model exists for the dilute solutions which can map these properties after a few parameters are determined from the existing data. This theoretical model, first proposed by Landau and Pomeranchuk,[3] is that an atom of He^3 added to superfluid He^4 should behave as an impurity with an ideal gas-like energy spectrum of

$$\epsilon = E_0 + \frac{p^2}{2m_0^*} \tag{2}$$

where E_0 is the binding energy of the He^3 atom to the surrounding He^4, p is the He^3 quasiparticle momentum, and m_0^* is the effective mass of the quasiparticle. As more He^3 atoms are added to the He^4, the binding energy and the effective mass of each quasiparticle begins to change slightly under the influence of the field set up by the He^3 already present. For instance, m_0^* becomes m^* and E_0 goes to E. In addition, a term of higher order than p^2 will contribute to the energy in (2) and is due to exchange scattering of the He^3 atoms. In a somewhat more physical picture, what has been done here is to replace each He^3 atom with a fictitious particle known as the He^3 quasiparticle. The He^3 atom actually interacts with both the He^4 and the other He^3 atoms, whereas the quasiparticle is now a particle interacting only with other He^3 quasiparticles. The effect of the He^3–He^4 interaction is now incorporated in m^* and ϵ, which are different than the bare He^3 atomic mass, m_3, and energy. Thus at low temperatures, where the number of He^4 phonons is extremely small, we can disregard the He^4. This is an especially attractive model for use with the dilution refrigerator, since in the refrigerator He^3 atoms diffuse through a nearly stationary He^4 bath. According to the theoretic model, we then replace the He^3 atoms by He^3 quasiparticles and dispense with the He^4 or replace it by a vacuum of 'ether'.[12] What we have is simple flow of the gas-like, free quasiparticles at a pressure π, which is actually the osmotic pressure of He^3 in He^4. A knowledge of the properties of this gas of He^3 quasiparticles would then allow us to analyse the refrigeration cycle.

The earliest attempts to calculate the thermodynamic properties of dilute He^3 solutions treated the He^3 quasiparticle gas as an ideal classical gas, which would have a molar specific heat at constant concentration or constant volume of $C_v = 3R/2$ and at constant pressure of $C_\pi = 5R/2$, where R is the gas constant. These results are valid only for temperatures much higher than the Fermi temperature given by

$$T_f = \frac{\hbar^2 (3\pi^2 N_A / v)^{2/3}}{2k_b m^*} \tag{3}$$

where $\hbar$ is the reduced Planck's constant, N_A is Avogadro's number, v is the volume per mole of He^3 in solution, and k_b is Boltzmann's constant. The behaviour of T_f is roughly as $X^{2/3}$ and is about 0·38 K at X = 6·4%. Obviously, degenerate effects must be taken into account for temperatures reached in the dilution refrigerator. The first approximation would neglect any interactions between He^3 quasiparticles. Such an approximation comes fairly close to experimental results for several properties. The best accuracy and internally consistent results occur only when weak interactions between He^3 quasiparticles are taken into account. Derivation of the effective mass and total energy

of the quasiparticles from theory alone requires a microscopic theory, which to date is not sufficiently accurate. Instead, a phenomenological theory by Bardeen, Baym, and Pines [23] (BBP) can be used to predict the variation of these two quantities with concentration and by relying on existing experiments, absolute values can be determined. BBP first suggested the interaction potential in momentum space of

$$V(k) = V_0 \cos(\beta k) \qquad (4)$$

to fit spin diffusion results,[24] with $\beta = 3{\cdot}16$ Å and $V_0 = -0{\cdot}0754\, m_4\, s^2/n_4 = 1{\cdot}303 \times 10^{-45}$ J cm^3, where m_4 is the mass of the He^4 atom, s is the velocity of first sound in He^4 at $T = 0$, and n_4 is the number density of pure He^4 at $T = 0$. Ebner [25] devised a slightly different potential which should be better for higher concentrations. The form of his potential is much more complicated than (4) and is not displayed here. All the thermodynamic properties described in this paper, and in much more detail in an earlier work,[11] are based on Ebner's potential. Improvements in $V(k)$ can be made to explain better some of the latest heat of mixing [26] and osmotic pressure [26,27] measurements. The interaction potential has a reasonably large influence in the low temperature limit on such properties of the He^3 quasiparticles as the energy and osmotic pressure. It has a much lesser effect on the effective mass, but it is responsible for the variation of effective mass with concentration. The interaction has essentially no effect on the specific heat and entropy providing the proper effective mass is used.

The details of calculating the thermodynamic properties of He^3 in He^4 using an interaction potential will not be given here. Such detailed calculations are discussed elsewhere.[11–13,28] Instead, a brief outline will be given of how the calculations are carried out, and then the important thermodynamic properties derived from these calculations will be discussed. An understanding of the dilution refrigerator only depends on these resultant properties and not on the methods used for calculation.

If the He^3 atoms were free particles, then all the thermodynamic properties would be just those of an ideal Fermi–Dirac gas as derived by Stoner.[29] When the interaction of the He^3 with the He^4 bath is turned on, then only two properties are affected; the internal energy at 0 K is shifted from $3RT_f/5$ by the amount E_0 and the effective mass changes from m_3 to m_0^*. The phenomenological theory of BBP requires that this shift in both the energy and effective mass be determined from experiment. The extrapolation of osmotic pressure and specific heat measurements to $X = 0$ gives the appropriate shifts in the energy and the effective mass, respectively. The BBP theory then predicts the additional shift in these two quantities as more and more He^3 is added to the solution and the He^3–He^3 interactions become important. The properties of an ideal Fermi–Dirac gas are still used, but with the appropriate effective mass, m^*, and the shift by E of the internal energy. Most existing experimental data agree quite well with these calculated properties. The specific heat of course still varies as T for $T \ll T_f$, but the proportionality constant depends on m^*/m_3. For $T \gg T_f$, the term C_v always approaches $3R/2$. The calculated osmotic pressure is shown in Figure 2. The value of π at $T = 0$ and $X = X_0 = 0{\cdot}064$ is $1{\cdot}63 \times 10^3$ N m^{-2} (12·2 torr), which is somewhat lower than the recently measured values of $(2{\cdot}24 \pm 0{\cdot}05) \times 10^3$ N m^{-2} (16·8 torr) by Landau et al,[22]

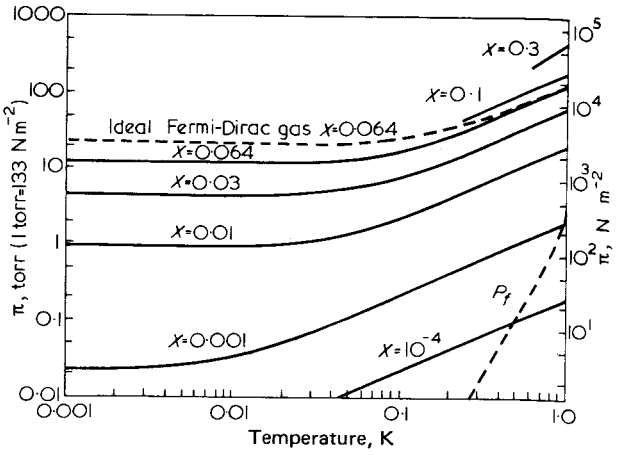

Figure 2. Calculated osmotic pressure of He^3 in liquid He^4 as a function of temperature for various He^3 concentrations. The curve P_f is the fountain pressure of pure He^4

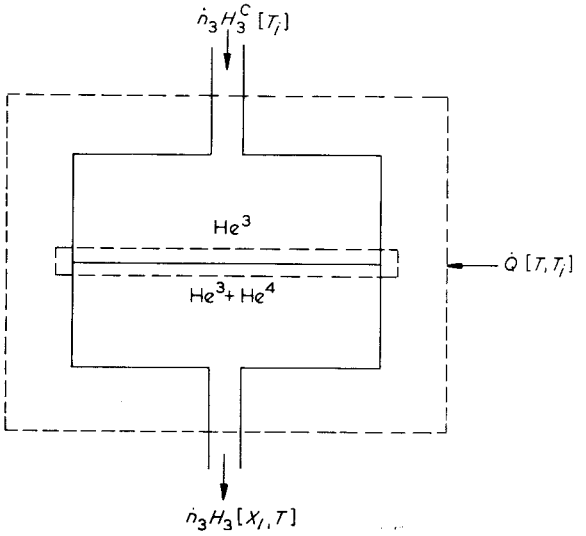

Figure 3. Schematic diagram of the mxiing chamber of a continuously operating dilution refrigerator

(2·30 ± 0·07) × 10^3 N m^{-2} (17·2 torr) by London et al,[30] abd 2·16 × 10^3 N m^{-2} (16·2 torr) by Ghozlan et al.[31] The difference, however, has little effect on the analysis of the dilution refrigerator. Other important thermodynamic properties are easily derived from the specific heat and osmotic pressure.

The continuous dilution process

Now let us consider the actual process of dilution as it takes place in the mixing chamber of a continuously operating dilution refrigerator under steady state conditions. A schematic of this process is shown in Figure 3. The quantity of interest is the heat absorption rate $\dot{Q}$. The simplest technique for evaluating $\dot{Q}$ is to treat the mixing chamber as an open thermodynamic system. Such a system is commonly treated by the engineer but is not very well-known to the physicist. The open system to be considered is shown by the outer dashed line completely enclosing the mixer. The system is considered an open system since mass is allowed

to enter and leave. Concentrated He^3 enters at a molar flow rate of $\dot{n}_3$, and the He^3 quasiparticle gas leaves at the same molar flow rate. The process is obviously analogous to the continuous vaporization of a liquid. Since no external work is being done by the system, and since there is no change in the internal energy of the system with time for steady state conditions, conservation of energy, or the first law of thermodynamics, for an open system is simply stated as

$$\dot{Q}(T, T_i) = \dot{n}_3 [H_3 (X_l, T) - H_3^c (T_i)] \qquad (6)$$

where $H_3 (X_l, T)$ is the molar enthalpy of He^3 along the lower phase separation line, and $H_3^c (T_i)$ is the molar enthalpy of He^3 in the incoming concentrated stream at a temperature T_i. For nearly pure He^3, the last term on the right becomes H_3^0, which for $T \leqslant 0{\cdot}04$ K is about equal to $12\,T_i^2$ J mole^{-1} K^{-2}. The term $H_3 (X_l, T)$ can be evaluated in principle from a table of values for $H_3 (X, T)$, but at temperatures below about 0·1 K the desired result is a small difference in two large quantities and, thus, cannot be found with sufficient accuracy. To get around this dilemma, we shall consider an alternative calculation of the heat absorption rate. Though exactly equivalent to (6), this second method gives a way of evaluating $H_3 (X_l, T)$ below 0·1 K much more accurately than the direct evaluation from a table of H_3 as a function of X and T. Consider now a second open thermodynamic system designated by the inner dashed lines in Figure 3 just around the phase boundary. Within this very limited system, temperature equilibrium exists, and the actual crossing of the phase boundary by He^3 is reversible. The total heat absorption rate in this reversible process is simply

$$\dot{Q}_t = \dot{n}_3 T\Delta S_3 = \dot{n}_3 T[S_3(X_l, T) - S_3^0 (T)] \qquad (7)$$

where S_3 and S_3^0 are the molar entropies of He^3 in the dilute and concentrated phases, respectively. But this total heat actually is coming from two places—the external heat that is being applied and the heat that is being conducted to the interface from the incoming warm He^3. Thus we write

$$\dot{Q}_t = \dot{Q} + \dot{n}_3 [H_3^0 (T_i) - H_3^0 (T)] \qquad (8)$$

and when combined with (7), this becomes

$$\frac{\dot{Q}(T, T_i)}{\dot{n}_3} = T[S_3(X_l, T) - S_3^0(T)] + H_3^0(T) - H_3^0(T_i) \qquad (9)$$

If we compare (9) with (6) and let $H_3^c = H_3^0$, we then note that

$$H_3(X_l, T) = H_3^0(T) + T[S_3(X_l, T) - S_3^0(T)] \qquad (10)$$

which says that the enthalpy in the dilute, quasiparticle 'gas', phase is simply the enthalpy of the quasiparticles in the strongly interacting, or pure liquid He^3, phase plus the heat required to 'vaporize' the quasiparticles into the 'gas' or weakly interacting phase Equation 10 is used to calculate $H_3(X_l, T)$ below 0·1 K, and for $T \leqslant 0{\cdot}04$ K the heat absorption rate of the dilution refrigerator according to (6) becomes

$$\frac{\dot{Q}(T, T_i)}{\dot{n}_3} = 94\,T^2 - 12\,T_i^2 \text{ J mole}^{-1} \text{ K}^{-2} \qquad (11)$$

For mixer temperatures considerably above the minimum, the heat exchangers will be quite efficient and T_i will be nearly equal to T. In this case the maximum heat absorption rate of $Q(T, T)/\dot{n}_3 = 82\,T^2$ J mole^{-1} K^{-2} He^3 is achieved. If X_0 were 0·068 instead of 0·064, the head absorption rate would be $78\,T^2$ J mole^{-1} K^{-2}. Figure 4 gives curves of $H_3 (X_l, T)$ and $H_3^0 (T)$, which can be used in (6) to find the heat absorption rate at higher temperatures. It is obvious from these curves that the incoming pure He^3 can be at a much higher temperature than the outgoing dilute He^3 and still provide refrigeration. From (11) we find that the refrigeration power goes to zero whenever $T/T_i = 0{\cdot}36$. This ratio decreases at higher temperatures to about 0·25 at $T = 0{\cdot}2$ K. The temperature at which the refrigeration power in a given refrigerator goes to zero is found from an analysis of the heat exchanger, as will be discussed later.

The actual processes which are involved to bring about the continuous dilution are shown schematically in Figure 5. The vacuum pump circulates nearly pure He^3 through the system and compresses the gas to a pressure in the range 25–200 torr. The total molar flow rate can be determined either with a commercial calorimetric flowmeter or by measuring the pressure drop across a known impedance inserted in the flow path at room temperature. If the pressure drop, ΔP, is much smaller than the absolute pressure, P, then the total flow rate is simple $\dot{n} \propto P\Delta P$, where the proportionality

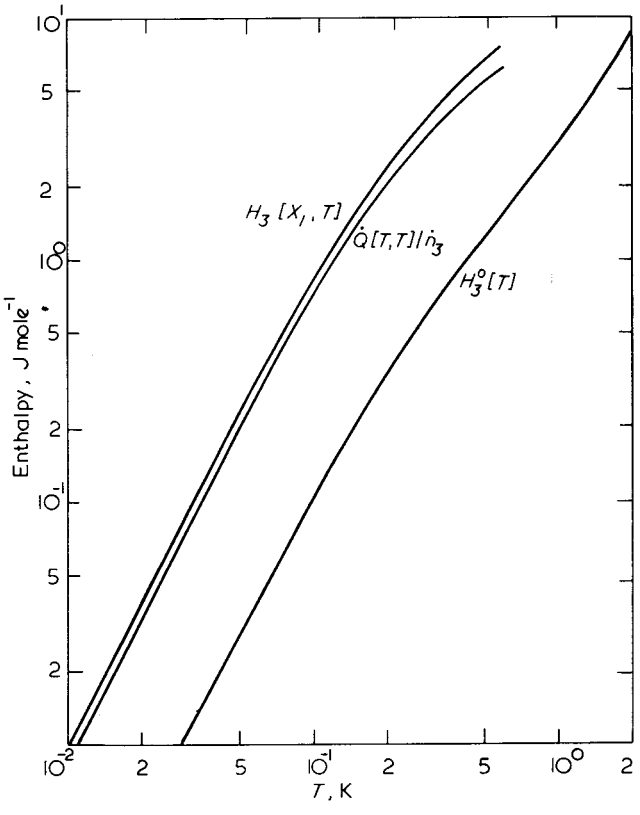

Figure 4. Enthalpy and heat absorption curves for calculation of mixer behaviour

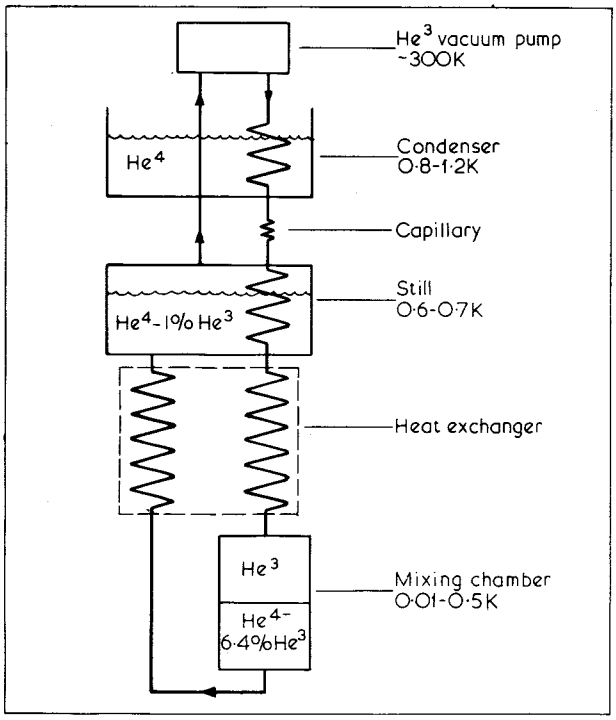

Figure 5. Schematic diagram of the He^3–He^4 dilution refrigerator

constant can be calculated from the impedance value. A useful feature of this second technique is that the value of ΔP is independent of P and is inversely proportional to the total flow impedance in the refrigerator, due primarily to the small capillary below the condenser. Such a relation is true if only liquid passes through the capillary (see next paragraph). A decrease in ΔP immediately signals a blocking of the capillary or that some gas is passing through it. The fraction of He^3 in the gas being circulated by the pump is usually determined with a mass spectrometer leak detector. This He^3/He^4 ratio can be a very useful bit of diagnostic information. At a pressure of 25–200 torr, the gas condenses in a condenser held at about 1 K by a pumped He^4 bath. Helium consumption is much more economical if the outside bath is left at 4·2 K and only a small pot inside the vacuum can, fed by a needle valve in the 4·2 K bath, is used for the 1 K stage. Progress has been made recently to either reduce the size of this pumped He^4 pot from several hundred cm^3, or to eliminate this stage altogether. If the pumped He^4 pot can be fed continuously at a rate equal to the consumption rate of helium, then there is no reason for a large reservoir. DeLong et al [32] have used a capillary between the 4·2 K bath and a pumped pot for a few cm^3 volume maintained at about 1·3 K. The capillary is of sufficient size to give a flow rate slightly higher than that needed for the expected maximum power input. With power inputs less than this critical value, the liquid level rises up the pumping tube to the point where the necessary additional heat is absorbed from the 4·2 K bath. It is possible to eliminate the He^4 pot entirely if a Joule–Thomson circuit for the He^3 liquefication is employed.[33] In this case the vacuum pump needs to be backed by a compressor to bring the pressure up to about 4 atm (0·4 MN m^{-2}).

After the He^3 is liquefied, either in a conventional condenser or by the Joule–Thomson technique, the pressure on the liquid is then reduced by passing through a capillary. There are two rather important points which need to be observed at this point. First the condensing rate of the empty condenser must be higher than the flow rate through the capillary. When this is so, the condenser begins to fill up and thus reduce the condensing rate due to a loss of condensing surface area. At some point, the condensing rate then equals the flow rate through the capillary and the condenser is running partially full. If the condensing rate is too small or the capillary impedance too small, then some gas will pass through the capillary and put a heat load on the still and possibly the warmer heat exchangers. One must also be careful to maintain the pressure in the still exchanger to at least the vapour pressure of He^3 at the still temperature, to prevent gas formation due to vaporization. This is usually done [13] by putting a second capillary below the still. It would be possible to place the entire impedance anywhere below the still, but above about 0·2 K, and yet have negligible viscous heating. However, it would not be wise to have much of a pressure drop in the He^3 stream below the still because of the temperature rise which occurs upon the isenthalpic expansion of the liquid. The general thermodynamic expression for the change in temperature with pressure in a constant enthalpy process is given by

$$\left(\frac{\partial T}{\partial P}\right)_H = -\frac{1}{C_p}\left[v - T\left(\frac{\partial v}{\partial T}\right)_P\right]$$

where C_p is the molar specific heat at constant pressure and v is the molar volume. For pure liquid He^3 at these low temperatures, the second term within the brackets in the above equation is negligible and C_p is essentially identical to C_3^0 for the low pressures used in a dilution refrigerator. Thus, we have the expression $(\partial T/\partial P)_H = -v_3^0/C_3^0$, which at 0·7 K has the value $-10\ \mu$K per (N m^{-2}) or $-1{\cdot}3$ mK $torr^{-1}$. At 0·2 K, these numbers are about 35% higher. A pressure drop below the still on the order of 100 torr ($1{\cdot}3 \times 10^4$ N m^{-2}) would then place a fairly heavy load on the following heat exchanger. The second capillary should then be designed to produce a pressure drop of the order of only 10 torr ($1{\cdot}3 \times 10^3$ N m^{-2}), which would allow the still to operate as high as 1 K before vapour formed in the still heat exchanger. Provided the second capillary is not thermally anchored to the still, any gas formation in this second capillary is of only small consequence, since it reduces the temperature of the He^3 stream and does not change the enthalpy. The only effect on the heat exchangers is then due to a reduced temperature difference available for the heat transfer. Usually the hydrostatic head below the second capillary is sufficient to suppress any gas formation there.

The He^3 liquid then enters the main heat exchanger and exits at a temperature T_i, which is the inlet temperature to the mixing chamber. A small amount of He^4 in the circulated He^3 will not have much direct effect on the behaviour in the mixer but it can in the heat exchanger. The effective specific heat [16] of solutions in the range 80–95% He^3 can be at least double that for pure He^3 for temperatures of 0·2–0·6 K. Thus He^4 circulation puts a much higher load on the warmer heat exchangers and leads to a higher mixer temperature. Use of an He^4 film surpressing still [34] permits He^3 concentrations of about 95% to be circulated, which is much higher than that usually attained with the conventional orifice type of still.

The driving process for dilution in the mixing chamber is brought about by the depletion of He^3 from the dilute solution in equilibrium with the pure He^3 phase. The depletion actually occurs in the still at about 0·7 K, where heat is applied to cause vaporization. Since the vapour pressure of He^3 is much higher than that of He^4 at this temperature, the gas given off is nearly pure He^3 which returns to the pump. As the He^3 is removed from the dilute solution in the still, He^3 diffuses through the stationary He^4 from the mixer to the still. Ideally, the He^3 diffusion, or He^3 quasiparticle gas flow, is at constant osmotic pressure, but any impedance in the heat exchangers causes some pressure drop. The osmotic pressure curves of Figure 2 show that for low mixer temperatures the concentration in the still at about 0·7 K will be approximately 1% He^3. Any osmotic pressure drop in the heat exchanger will reduce this concentration and cause an increase in the amount of He^4 evaporated in the still. However, pressure drops of the order of 1–5 torr should not significantly increase the He^4 circulation. The flow of cold He^3 quasiparticle gas from the mixer to the still is utilized by the heat exchanger to cool the incoming pure He^3 liquid. The specific heat that is being used in the dilute side of the heat exchanger is the specific heat at constant osmotic pressure, or more exactly, at constant μ_4. This calculated specific heat is shown in Figure 6. The various mixer temperatures T_m represent different osmotic pressures. The limiting low temperature behaviour of $C_{\mu 4} = 107{\cdot}2\,T$ J mole^{-1} K^{-2} is just C_v for a 6·4% solution. The $5R/2$ behaviour at higher temperatures is just that of an ideal classical gas at constant pressure. The fairly rapid rise in $C_{\mu 4}$ at the highest temperatures is a result of the rapidly increasing fountain pressure reducing the equilibrium concentration. The high initial values of $C_{\mu 4}$ for the high mixer temperatures are due to the He^3–He^3 interactions becoming fairly strong at the high concentrations present at these high mixer temperatures. Fortunately, $C_{\mu 4}$ is much higher than C_3^0 at all temperatures, for if the opposite were true, the dilute stream would have little cooling power on the incoming pure He^3

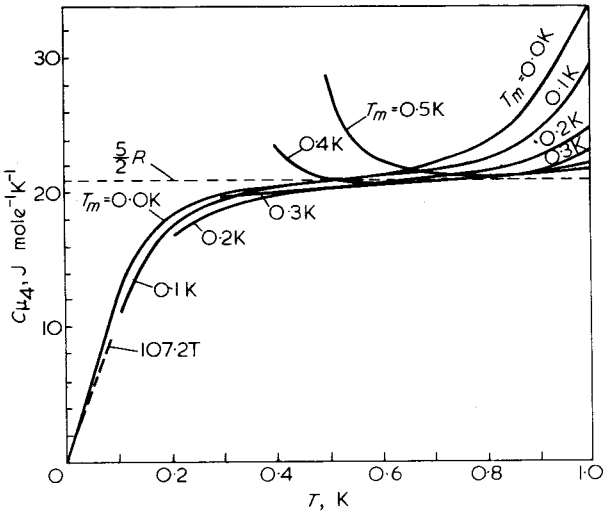

Figure 6. Calculated specific heat of He^4 at constant μ_4

The single-cycle dilution processes

Several techniques exist whereby the refrigerator may be operated for a certain period of time without the need of cooling incoming warm He^3. These are known as one-shot, or single cycle, processes and produce temporary refrigeration from a reservoir of He^3. Vilches and Wheatley [10] reached about 4·5 mK with the more common of these one-shot processes (simply stopping the return He^3 flow in the continuous process) and maintained that temperature about an hour before depleting the He^3 reservoir. This low temperature limit is in rough agreement with the calculated expression [13]

$$T_m = (4\,m\,K)\,d^{-1/3} \tag{12}$$

where d is the diameter of the exit tube in mm. This expression is derived by considering the viscous heating of the dilute He^3 passing through the exit tube and the conduction of this heat back to the mixer through the liquid stream. Such a temperature serves as the lower limit one might hope to reach in a continuous refrigerator with nearly perfect heat exchange between the concentrated and dilute streams.

The mixer behaviour in all of the one-shot processes is derived by again considering the mixer to be an open thermodynamic system. The time rate of entropy change for the total system is then

$$\dot{S}_t = \frac{\dot{Q}}{T} + \dot{n}_3 S_3 + \dot{n}_4 S_4^0 \tag{13}$$

where n_3 and n_4 are the molar flow rates of He^3 quasiparticles and of pure He^4 into the mixer. Note that these are externally measured flow rates. The total system entropy is expressed as

$$S_t = n_d S_d + n_3^0 S_3^0 \tag{14}$$

where n_d is the number of moles of dilute solution with entropy S_d and n_3^0 is the number of moles of pure He^3 present at entropy S_3^0. In almost all situations of interest, the term $n_d S_d$ is just $n_{3d} S_3$, where n_{3d} is the number of moles of He^3 in the dilute solution. Equations 13 and 14 can be used to describe any one-shot process. Two single cycle techniques exist, which we shall call (i) the He^3 removal and (ii) the He^4 input processes. Each of these, in turn, can pass through two different stages – one where a pure He^3 phase is present and the other where it is not. The He^3 removal process, with the pure He^3 phase present, as mentioned previously, is the more common. In that situation $\dot{n}_4$ in (13) is zero. Combining (13) and (14) along with the fact that $n_3 = \dot{n}_{3d} + \dot{n}_3^0$ leads to the equation

$$\frac{dT}{d(n_3^0/n_0)} = \frac{\dot{Q}/\dot{n}_3^0 + (S_3 - S_3^0)T}{(n_3^0/n_0)C_3^0 + (n_{3d}/n_0)C_3} \tag{15}$$

where C_3^0 and C_3 are the He^3 molar specific heats in the pure and dilute phases and $\dot{n}_0$ is the moles of He^3 originally in the pure phase. For isothermal behaviour we simply have

$$-\frac{\dot{Q}}{\dot{n}_3^0} = (S_3 - S_3^0)T \tag{16}$$

where the right side is just 82 T^2 J mole^{-1} K^{-2} for T $T \leqslant 40$ mK. Note that the molar flow rate involved is n_3^0, the rate He^3 is passing across the phase boundary, and is a

negative number for He^3 leaving the concentrated phase. This flow rate is different [35] than the flow rate $\dot{n}_3$, leaving the mixer and entering the pump, because some of the pure He^3, along with a back flow of He^4, is used to produce additional dilute solution to replace the volume of concentrated solution removed. The two flow rates are related by the expression

$$\dot{n}_3^0 = \frac{\dot{n}_3}{1 - \frac{v_3^0}{v_3}} \qquad (17)$$

where v_3^0 and v_3 are the molar volumes of He^3 in the pure and dilute phases. For $T \leqslant 0{\cdot}1$ K we get $\dot{n}_3^0 = 1{\cdot}091\,\dot{n}_3$. Experimentally,[10] the one shot refrigerator could absorb $(83 \pm 4)T^2$ J mole^{-1} K^{-2}, but it is not clear whether $\dot{n}_3$ or $\dot{n}_3^0$ was used to arrive at such a number. The over-all transient behaviour of the He^3 removal process can only be found from a numerical solution of (15). The results of such a solution are shown in Figure 7. The initial conditions used for these calculated results were those used for the experimental results, also shown in Figure 7. Agreement between the two sets of curves is good. Theoretically, it should be possible to reach the lower limit, given by (12), starting with the mixer at 0·3 K, but the one attempt [35] reached only 27 mK before depleting the He^3 reservoir. The reason for this discrepancy is unclear. After the pure He^3 phase is depleted, the second stage of the He^3 removal process is entered. This stage, called 'extraction cooling', has been observed,[35] but appears to have little practical importance. The reader is referred to reference 11 for additional details.

The He^4 input process for one-shot operation has the advantage of not being limited by viscous heating of the flowing liquid because the He^4 is superfluid. A superleak is necessary to add the He^4 in a reversible manner.[36] A successful amount of cooling using this process has not been achieved, but it has the potential for reaching temperatures in the range of a few tenths millikelvin.[11,37] An ingeneous suggestion by Edwards [37] shows how to use a continuous dilution refrigerator both as a pre-cooling stage and as a source of He^4 to be fed through a superleak to a separate He^3 chamber.

Heat exchangers

The lowest temperature which can be reached in a continuously operating dilution refrigerator is determined by the quality of the heat exchangers. Until recently, a detailed study of heat exchangers had not been done, except for practical schemes of increasing the surface area. The most common of these schemes has been the use of sintered copper powder [13] or of closely spaced copper foils [38] in a series of copper blocks connected by small tubing. Obviously, by increasing the size and number of these heat exchangers, excellent heat transfer and very low temperatures can be achieved. The disadvantage is that long times will be required to condense and cool-down the large amount of He^3 and He^4 in the system. Also, equilibrium times for a change in mixer temperature are increased. The use of smaller optimal heat exchangers cuts down on some of this 'dead' time and makes the refrigerator more productive. The theoretical groundwork for the design of more nearly optimal exchangers is near completion, but the practical developments may be just beginning.

Only the case of zero heat input to the mixer is considered here since the desirable low temperature limit usually imposes the most stringent requirements on the heat exchangers.

Classification. In discussing heat exchangers, we need some scheme of classification for the different possible types. The terms continuous and discrete have had widespread use. Here we define a continuous exchanger as one in which there are no discontinuous changes in physical parameters between points at two different temperatures, for example, co-axial Cu–Ni tubes between the still and mixer. The temperature gradients are then continuous functions of position. A discrete exchanger is one which is isolated from the end points by relatively low heat conductance paths, for example, a sintered copper exchanger connected via small diameter Cu–Ni tubes. Whether a particular heat exchanger should be used in a continuous or discrete fashion depends on the heat conductances in the axial direction along the liquid streams and the body walls. Only when this heat conductance is small compared with the total heat transferred should it be used in a continuous manner. In quantitative terms, this condition is expressed by

$$Y = \sum_j Y_j \equiv \sum_j \frac{\kappa_j A_j}{L_j \dot{n}_3 C_j} \ll 1, \qquad (18)$$

where κ is the thermal conductivity, A is the cross-sectional area, L is the total length, and C is the He^3 molar specific heat. The index j takes on the three subscripts, c, d, and b, which refer to the concentrated and dilute liquid streams, and the body material, respectively. However, C_b is not the specific heat of the body, but should best be given the value of C_d. The term C_d is the same as the specific heat $C_{\mu 4}$ discussed earlier. We may substitute into (18) the approximate value

$$B_j = \kappa_j / C_j \simeq 4 \times 10^{-5} \text{ mole s}^{-1} \text{ cm}^{-1} \quad j = c, d \qquad (19)$$

We define an ideal continuous exchanger as one in which Y is zero; or in terms of the axial thermal conductance, $K = \kappa A/L$, this condition may be represented by the expression

$$(K_b, K_l) = (0, 0) \qquad (20)$$

where the subscript l refers to both liquid streams.

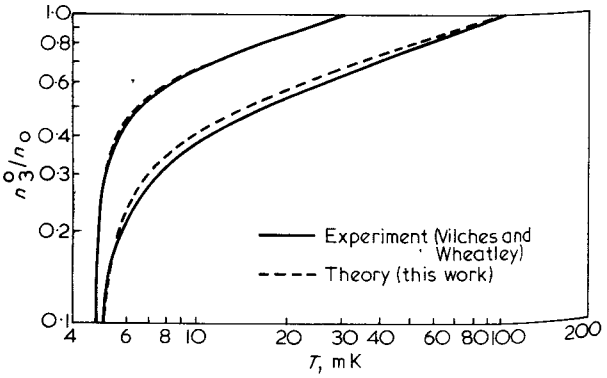

Figure 7. Calculated temperature dependence of the fraction of pure He^3 phase remaining in the mixing chamber of a one-shot dilution refrigerator compared with experiment [10]

Whenever (18) does not hold, it is then best to break the exchanger into one or more isolated segments (discrete heat exchangers) to reduce the axial heat flow. The larger the value of Y, the more segments required to achieve the desired mixer temperature. The upper limit on the required number of segments is reached when the liquid and/or body conductivity becomes large. This limit is expressed quantitatively as

$$W_j \equiv \frac{\kappa_j A_j \rho_j}{L_j \sigma_j} \gg 1 \quad j = c, d, b \tag{21}$$

Here ρ is the Kapitza resistivity and σ is the heat transfer surface area in the exchanger. Again, we require that ρ_b and σ_b be given the values ρ_d and σ_d. It is unfortunate that neither Y nor W_j alone is the ideal parameter to use for both the high and low conductivity limits, although W_j is used over the whole range with fairly good success later in this paper. Unlike (18), it is possible for (21) to be satisfied in several different ways. However, to simplify the classification, we treat the two liquid streams together and consider the cases where W_b and/or W_l are infinite. Expanding on the representation in (20), we might represent the four extremes in heat exchanger behaviour in the following manner:

$$(K_b, K_l) = \begin{pmatrix} 0,0 & 0,\infty \\ \infty,0 & \infty,\infty \end{pmatrix} \tag{22}$$

keeping in mind that the test for zero behaviour is with the value of Y_b or Y_l and the test for infinite behaviour is with W_b or W_l. Equation 22 may be thought of as representing the four corners of an entire surface of heat exchanger behaviour. The performance might be characterized by the parameter

$$\epsilon \equiv \frac{T_{ci} - T_{co}}{T_{co}} \tag{23}$$

where T_{ci} and T_{co} are the inlet and outlet temperature of the concentrated stream in the exchanger. Note that the parameter ϵ defined here is entirely different than the well-known heat exchanger effectiveness, which is the ratio of the actual heat transferred in a given exchanger to the maximum possible rate of heat exchange, that is, with an ideal continuous exchanger of infinite surface area. Use of the parameter ϵ from (23), rather than effectiveness, simplifies the heat exchanger calculations and discussions. The relative behaviour of the various types of heat exchangers can be visualized in Figure 8. In this figure the elevation of the surface represented in (22) is given by ϵ/σ, where σ is the heat transfer surface area. The flow rate, $\dot{n}_3$, is held fixed. Note that the $(0, \infty)$ corner has the same behaviour as the (∞, ∞) corner. This is so because the body in the $(0, \infty)$ case will be maintained at a constant temperature throughout by the liquid and thus behave no differently than if the body had infinite conductivity.

The behaviour of the most general type of heat exchanger, that is, one on the interior surface in Figure 8, can in principle be calculated, but with considerable effort. It is probably sufficient, however, to examine only the cases in the immediate vicinity of $(0, 0)$ and those along the $K_b = \infty$ edge in detail. In these cases the heat exchanger behaviour is found by solving, numerically, two coupled differential equations of the form:

$$A_l\left[\kappa_l \frac{d^2T}{dx^2} + \frac{d\kappa_l}{dT}\left(\frac{dT}{dx}\right)^2\right] - \frac{d\sigma}{dx}\int_{T_b}^{T}\frac{dT}{\rho}$$

thermal conduction — Kapitza conduction

$$+ \eta \nu_3^2 \dot{n}_3^2 \frac{dz}{dx} = \dot{n}_3 C_3 \frac{dT}{dx}$$

viscous heating — enthalpy change (24)

where $d\sigma/dx$ is the surface area per unit length, η is the viscosity, ν_3 is the volume of solution per mole of He^3, and dz/dx is the flow impedance per unit length. Other symbols have been defined previously. Temperatures are assumed to be uniform in the direction perpendicular to the flow, and the viscous heating term is neglected for the time being. Details of the calculations are discussed by Siegwarth and Radebaugh.[39]

Continuous heat exchangers. The results of calculations for the ideal continuous heat exchanger, or the (0, 0) case, are shown in Figure 9 for three difference values of Kapitza resistivity. The curves are valid for the case of 95% He^3 on the concentrated side.[39] A concentration of 90% He^3 would raise the curves about 2%. The still temperature can be varied between 0·5 and 1·0 K with less than 1% effect on the curves. For $\sigma_d/\sigma_c = 1$, the curves are raised by about 4%, and at $\sigma_d/\sigma_c = 2$ the curves are lowered by 1·4%. Thus little is gained by increasing σ_d only, since the dominant resistance is due to ρ_c. Those interested in the curves off to the right of Figure 9 can use the relation

$$T_m = a\left(\frac{\sigma_c}{\dot{n}_3}\right)^{-1/2} \tag{25}$$

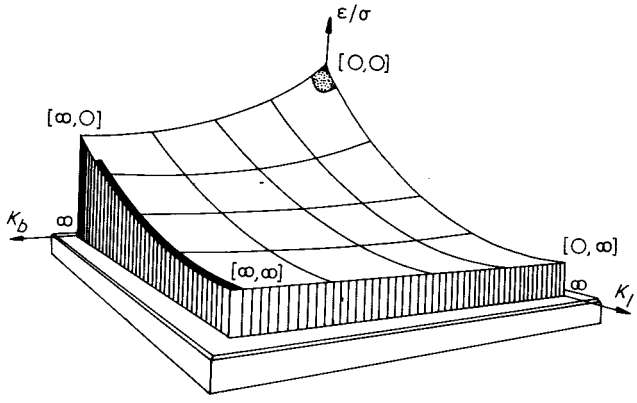

Figure 8. A qualitative sketch of the heat exchanger performance parameter ϵ, per unit surface area, σ, in the plane of axial thermal conductance, K, for both the body and liquid. The lightly shaded area shows the region where a continuous exchanger may be used and the two solid black areas indicate the position of most exchangers used presently. The four corners are represented by the four extremes in the quantity (K_b, K_l)

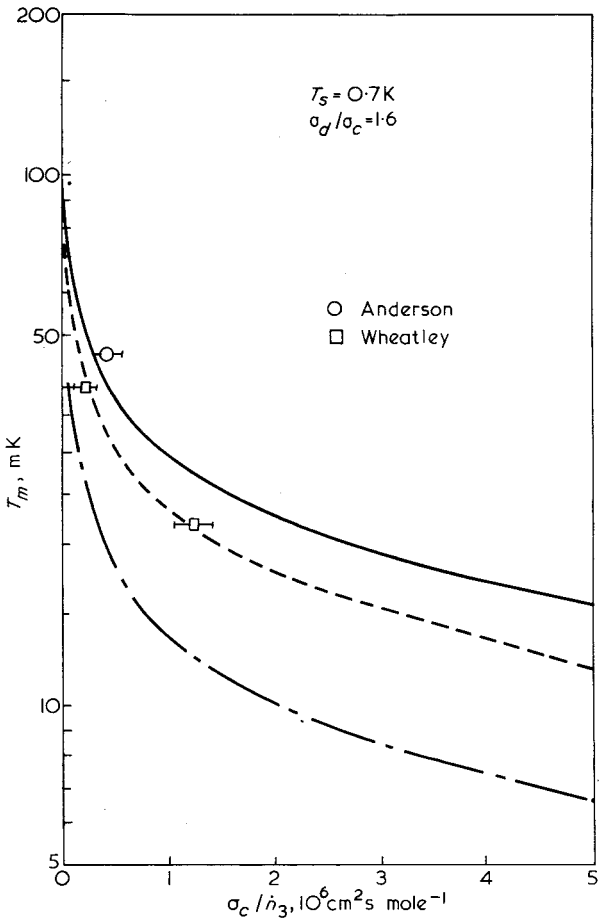

Figure 9. Minimum mixer temperature as a function of the concentrated stream surface area divided by He^3 flow rate for an ideal continuous heat exchanger. The upper curve is for ρ_c and ρ_d the same as for copper. The middle curve is for ρ_c and ρ_d reduced by the factor 1·8, and the lower curve is for a reduction factor of 20/3. The experimental points are from Anderson [40] and Wheatley [41]

where a depends on the heat exchanger material. Approximate values of a in units of (K cm $s^{1/2}$ mole $^{1/2}$) are: copper, 36; Cu–Ni, 27; and plastic, 15. Equation 25 should hold to better than about 5% for $T_m < 15$ mK. Equation 25 also follows from Neganov's [40] equation (22). In fact, he very nicely analysed dilution refrigerator exchangers and presents an equation for the behaviour of any type of heat exchanger. However, the equation has certain limitations when applied to discrete exchangers, and for both discrete and continuous exchangers it becomes difficult to use accurately when the concentrated He^3 stream is above about 0·1 K. The reason is that H_3^0 is no longer even approximately proportional to T^2.

Also shown in Figure 9 are two sets of experimental data points [41,42] obtained with co-axial Cu–Ni tubing heat exchangers. These two exchangers have a value of Y in (18) of about 10^{-3}; thus, they can essentially be considered ideal continuous exchangers. The point of Anderson [40] is above the calculated curve and is probably because T_m was measured outside the mixing chamber. Both points of Wheatley [41] (taken with two different flow rates) agree very well with the middle curve and suggest that the Kapitza resistance to the Cu–Ni tubes is about 1·8 times smaller than to copper. (Additional points just published by Wheatley et al,[63] also agree with the middle curve.) The Kapitza resistance to Epibond 100A,[43] and probably most plastics, is about a factor of 20/3 smaller than to pure copper, so T_m would be given by the lower curve in Figure 9. The ordinate on this curve is simply shifted by a factor of 20/3 from the upper cruve. Thus, plastic appears to be an especially attractive material for improved heat exchangers of the future. The first to consider plastic heat exchangers for the dilution refrigerator was probably Sydoriak.[44]

As one moves out on the K_l axis away from the (0, 0) corner, the thermal conduction term in (24) must be included. However, it has been shown [39] that even for values of Y_l as high as 0·2, the resultant mixer temperature can be determined accurately to better than 6% simply by multiplying the mixer temperature of the ideal continuous exchanger by the quantity $(1 + Y)$. This should be nearly true even for Y composed entirely of Y_b. For much higher values of Y, the curve is no longer dependent solely on Y and $\sigma_c/\dot{n}_3$. However, there appears to be little practical demand for exchangers which have $Y > 0{\cdot}2$ but which still are not in the region of $K_b = \infty$.

Discrete heat exchangers. Analysing discrete heat exchanger along the $K_b = \infty$ edge is much more complicated than for the ideal continuous exchanger. The behaviour depends on additional parameters, such as the number of segments (copper blocks) and the distribution of the total surface area among the various segments. First we consider the case of a set of perfect discrete heat exchangers, that is, each segment contains an infinite surface area. The behaviour is determined [28] directly from an enthalpy balance between the dilute and concentrated streams and is shown in Figure 10 for various concentrated stream inlet temperatures. For the inlet temperatures of 0·05, 0·1, and 0·2 K, there is negligible difference between the pure He^3 and 95% He^3 cases. These curves show that at least four exchangers are required to reach 10 mK for $T_i = 0{\cdot}7$ K, but that if a continuous exchanger is used to give $T_i = 0{\cdot}1$ K, then a minimum of two discrete exchangers are required. The exchanger temperatures as well as the mixer temperature behave approximately as $e^{-n/1{\cdot}38}$, where n is the number of exchangers. This relationship means that the temperature ratio of the j-1 to the jth exchanger, given by

$$\delta_p \equiv \frac{T_{j-1}}{T_j} \equiv \left(\frac{T_{ci}}{T_{co}}\right)_p \tag{26}$$

is nearly constant. The subscript p refers to the perfect discrete exchanger, and T_{ci} and T_{co} are the concentrated stream inlet and outlet temperatures, respectively. The value of δ_p depends somewhat on temperature and also on the mixer temperature. In most cases we can use the value $\delta_p \simeq 2{\cdot}3$ for the last exchanger when $T_{co} \leqslant 0{\cdot}025$ K. For all other exchangers we have

$$\delta_p = 2{\cdot}1 + 6T_{co} + 20T_{co}^2 \quad T_{co} < 0{\cdot}2\ \text{K} \tag{27}$$

where T_{co} is in K.

For any real heat exchanger, discrete or continuous, we might define the term δ as

$$\delta \equiv \frac{T_{ci}}{T_{co}} \tag{28}$$

which for a real discrete heat exchanger will be less than δ_p at the same T_{co}. The term ϵ, defined in (23), is then

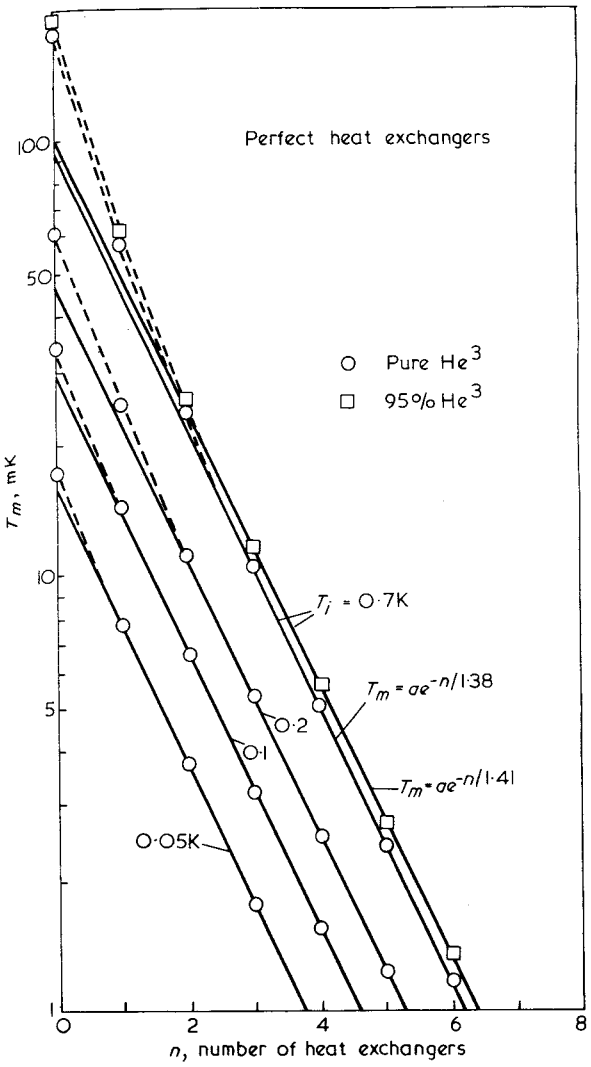

Figure 10. Calculated mixer temperatures as a function of the number of perfect discrete heat exchangers for various concentrated stream inlet temperatures

related to δ by the equation $\epsilon = \delta - 1$. For discrete exchangers near the $K_b = \infty$ edge, a measure of how well the exchanger is performing relative to a perfect discrete exchanger is given by the relative effectiveness, R, defined here as

$$R \equiv \frac{\epsilon}{\epsilon_p} = \frac{\delta - 1}{\delta_p - 1} \qquad (29)$$

For a given surface area, the value of R will depend on where along the $K_b = \infty$ edge the discrete exchanger is located. For the sintered copper or copper foil exchangers commonly used, W_c, W_d, and W_b each have values of at least 1 and usually much higher for exchanger temperatures around 50 mK and below. But, at about 0·1 K or higher, W_l may be the order of or even less than 0·1. A value of W_l of 0·1 gives a behaviour about midway between the 0 and ∞ liquid conductivity cases. Thus, presently used discrete exchangers range from the (∞, ∞) corner for the coldest exchanger and begin to approach the $(\infty, 0)$ corner for the warmest exchanger. The solid black areas in Figure 8 show this region, as well as the region where most continuous exchangers are located.

The behaviour of discrete exchangers at the (∞, ∞) corner is determined from a set of algebraic equations which equate the heat flow across the body wall to the enthalpy changes in the two streams.[39,40] The behaviour anywhere else along the $K_b = \infty$ edge is found from solving the differential equations in (24). Figure 11 shows the calculated [39] temperature profiles of a typical discrete exchanger ($W_d \simeq 7$; $W_c \simeq 3{\cdot}4$) and also the profiles for the case where κ_l is set to zero for the same exchanger. The mixer temperature was held at 10 mK for both cases. Note that with high values of W, most of the temperature changes in the streams occur in the small interconnecting tubes just prior to entering the exchanger. The figure also shows that the $\kappa_l = 0$ case produces a much greater total temperature change in the liquid streams, which means a higher value of ϵ/σ. However, this case still has a lower ϵ/σ than does the ideal continuous exchanger of the (0, 0) corner (see Figure 8). A proposed [39] means of making all presently designed discrete exchangers approach the $(\infty, 0)$ corner, and thereby improving their performance, is by inserting within the exchangers a few partitions, each containing a small hole, such that (18) will hold for the liquid streams in the hole. A drawing of one side of such an exchanger is shown in Figure 12. Because of the high Kapitza resistance, the partitions allow the liquid in one compartment to be thermally isolated from the liquid in the adjacent compartment. With three or four partitions, an exchanger which originally behaved like the (∞, ∞) extreme can be made to approach the $(\infty, 0)$ behaviour quite closely. Thus for the

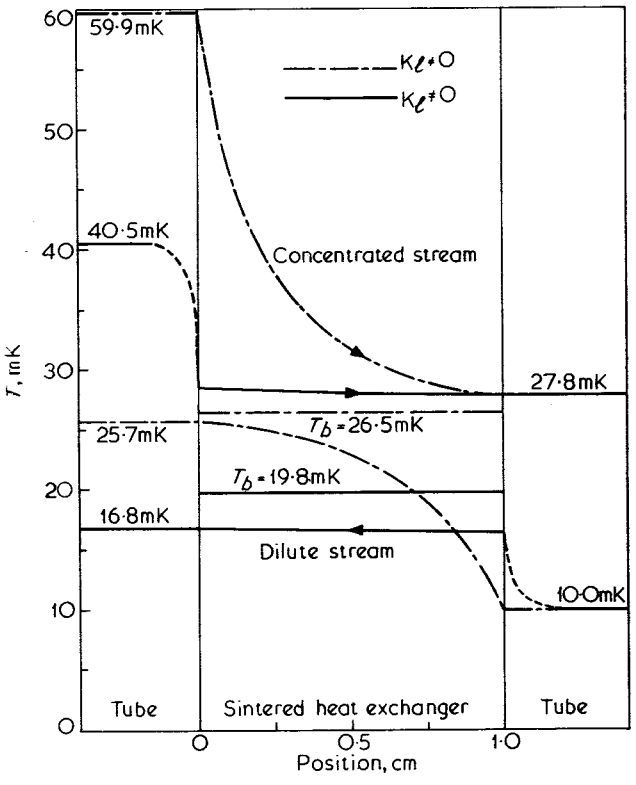

Figure 11. Calculated liquid and body temperature profiles within and just outside a typical discrete type heat exchanger for a mixer temperature of 10 mK. One set of curves is for a liquid conductivity, κ_l, of zero, and the other set is for the correct values of κ_l. The liquid volume on the concentrated side is 0·85 cm^3, and the dilute liquid volume is 2·1 times as large. The surface area per unit liquid volume is 400 cm^{-1}

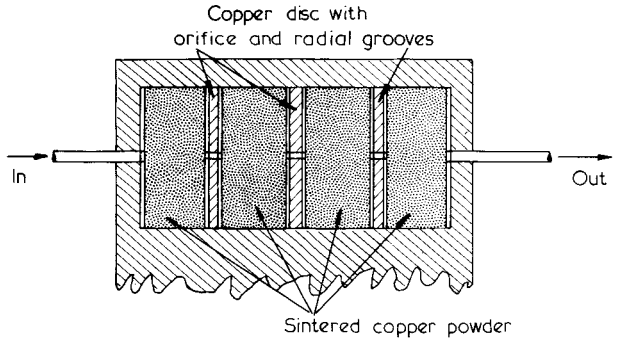

Figure 12. One side of a discrete heat exchanger with partitions for reducing liquid conductance. The radial grooves prevent a high flow impedance. The thickness of the discs might typically be approximately 1 mm and the orifice slightly smaller than the diameter of the interconnecting tubing

same ϵ, the surface area can be decreased a factor of three or even more, depending on the value of R. Of course, the partitions are of little use for exchangers which already have a small liquid conductance.

The maximum heat transfer within a discrete exchanger occurs [39] when 85 mole % of the total He^3 is on the concentrated side and 15 mole % on the dilute side, provided the surface areas per unit volume are equal on the two sides. These figures correspond to a ratio of 2·1 for the dilute to concentrated stream volumes in the lowest exchanger. The optimum ratio increases for the warmer exchangers because of the decreased concentration in the dilute stream at high temperatures. All the analyses discussed here for discrete exchangers are for this optimum ratio of volumes.

The design of an optimum set of discrete heat exchangers is carried out as follows. With a concentrated stream temperature of T_{ci} at the inlet to the exchanger, we choose a desired mixer temperature, T_m. The number of discrete exchangers is chosen to be equal to or greater than the minimum indicated in Figure 10. A larger number of exchangers requires less total He^3, but increases the complexity and the possibility of a leak. A suitable compromise must be chosen by the designer. The value of δ for each exchanger must be such that

$$\delta_1 \delta_2 \ldots \delta_n = \frac{\gamma T_{ci}}{T_m} \qquad (30)$$

where γ is the ratio of T_m to T_{co} of the nth exchanger and has the value 0·36 for $T_m \leqslant 0{\cdot}04$ K. A possible way of choosing the various δs is to make them all equal, or, perhaps, to make all the Rs equal. Such a choice takes a somewhat larger quantity of liquid than for an optimum combination of Rs. For all Rs between about 20% and 90%, the total surface area has a broad minimum for various combinations of R. The minimum does occur when the value of R is lowest for the coldest exchanger and highest for the warmest exchanger. Typical optimum values of R for a set of three exchangers could be 40%, 65% and 88%, but for all $R < 90\%$ these numbers could be changed by 10% with only a few percent increase in the liquid volume required. Of course, the combination must be such that (30) holds.

The proper values of R, so chosen, are now used with Figures 13 a or b, taken from preliminary work of Siegwarth and Radebaugh, to find the surface areas required on the concentrated side in each discrete exchanger made of copper. The surface area required on the dilute side varies

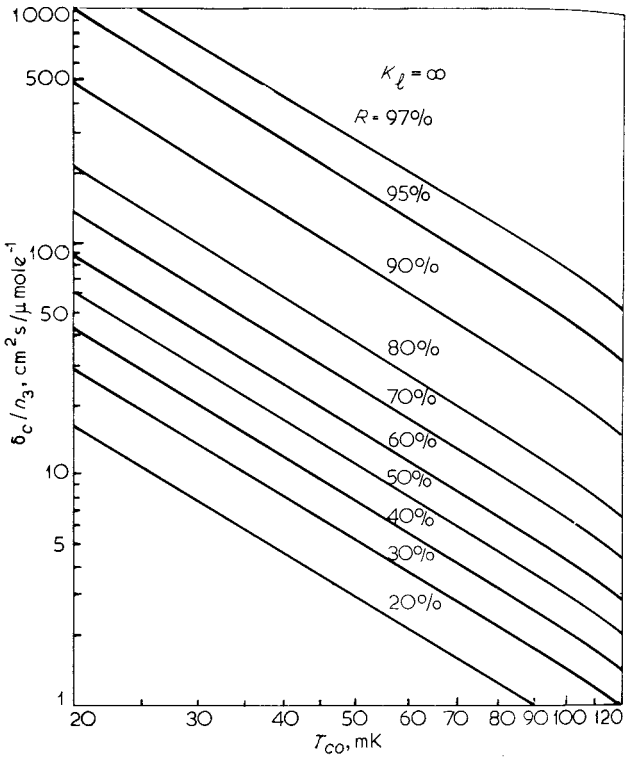

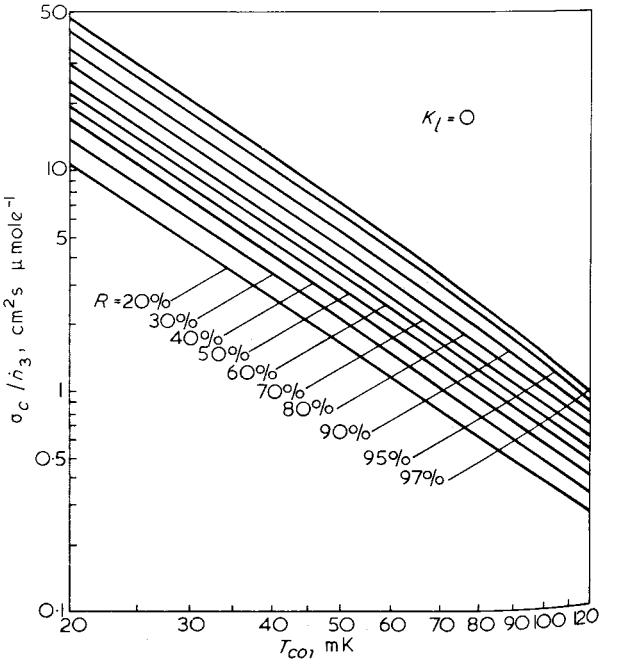

Figure 13. a The ratio of concentrated side surface area to He^3 flow rate required in a single discrete heat exchanger as a function of the concentrated stream outlet temperature, T_{co}, for various values of R, the relative effectiveness. The curves are for the case of infinite liquid conductance, or $W_l = \infty$. For $T_{co} < 20$ mK, all curves behave as $\sigma_c/n_3 \propto T_{co}^{-2}$

b The same curves as in Figure 13 a, except that these are for a discrete exchanger which has zero liquid conductance, or $Y_l = 0$. These curves also behave as $\sigma_c/n_3 \propto T_{co}^{-2}$ for $T_{co} \leqslant 20$ mK

from about 2·1 to 2·7 times the surface area on the concentrated side as T_{co} varies from 20 to 100 mK. Figure 13 b is for (∞, 0) exchangers. For most real exchangers in which three or four partitions are used in the lower exchangers, Figure 13 b may be used; but since K_l for these real exchangers is finite, about 10–20% additional surface area should be added to the value derived from the figure for an R value of 0·2%. As R is increased to 0·8, the additional surface area increases to 20–50%. For intermediate values of W_c and a given $\sigma_c/\dot{n}_3$ and T_{co}, the value of R will be somewhat between that given in Figures 13 a and b. If we define $r = (R - R_\infty)/(R_0 - R_\infty)$, where R_0 and R_∞ are the values of R for 0 and ∞ conductance, then $r \simeq 0{\cdot}95$, 0·5, and 0·1 for W_c of 0·01, 0·1, and 0·1, respectively. The curves in Figures 13 a and b are based on Kapitza resistance measurements between pure He^3 and electro-polished copper [43] and measurements between saturated He^3–He^4 solutions and non-electropolished copper.[13] The thermal boundary resistance which occurs in actual heat exchangers, usually annealed in a hydrogen atmosphere, could be different, although the long phonon wavelengths at these temperatures should make the Kapitza resistance rather insensitive to surface condition, unlike the case at higher temperatures. Results in our laboratory show that the boundary resistance below 0·1 K between −325 mesh sintered copper powder (av particle dia = 27 μm) and a saturated He^3–He^4 solution is such that an 'effective' surface area of about 1 000 cm^2 per cm^3 of liquid is realized with a 40% packing fraction. Smaller particle sizes give smaller 'effective' surface areas. Considerably more work is needed on this subject. In any case, if future measurements give different resistances than those used in the calculations for Figures 13 a and b, the required areas shown in these figures need only be scaled in proportion to the boundary resistance.

For a mixer temperature of T_m, the value of T_{co} to use in Figure 13 for the lowest exchanger is just $T_{co} = T_m/\gamma \simeq T_m/0{\cdot}36$. For that exchanger, the term $(\delta - 1)$ is calculated from (29) using $\delta_p \simeq 2{\cdot}3$ and the desired value of R. From (28), the inlet temperature T_{ci} is found, and this is the value of T_{co} to be used in Figure 13 for the next exchanger. The proper value of δ_p to use for the succeeding exchangers is given by (27).

A typical example may have T_m = 10 mK and a heat exchanger inlet temperature of 0·2 K. This inlet temperature is achieved with a continuous exchanger designed to give a T_m of 0·2 γ K = 70 mK, which from Figure 9 requires a $\sigma_c/\dot{n}_3$ of 0·05 cm^2 s μmole^{-1}. A set of Rs for three discrete exchangers which is consistent with (30) and gives approximately the minimum liquid volume is 40%, 65%, and 88%. Values of $\sigma_c/\dot{n}_3$ required are then about 11, 7, and 2·4 cm^2 s μmole^{-1} for the coldest to warmest exchangers. Note the rapid decrease in size for each succeedingly warmer exchanger. For $\dot{n}_3$ = 20 μmole s^{-1} and a surface area per liquid volume of σ/V = 1 5000 cm^{-1}, the warmest exchanger contains only 0·032 cm^3 liquid on the concentrated side. One more discrete exchanger would have a volume comparable to that in the interconnecting tubes, and so it then would be wise to use a continuous exchanger instead of the discrete exchanger for higher temperatures. The continuous exchanger has no theoretical advantage in ϵ/V at higher temperatures except that the over-all value of σ/V of the discrete exchanger is reduced considerably when the volume of the interconnecting tubes are included in V.

Reduction of liquid volumes. We now turn to the question of obtaining the maximum ϵ/V for any heat exchanger. Values of the quantity ϵ/σ can be determined from the previous discussions and are shown qualitatively in Figure 8. For most co-axial tube exchangers, we have $\sigma/V \simeq$ 80 cm^{-1} for the concentrated side, whereas in sintered copper or copper foil exchangers this ratio may be as high as 1 500 cm^{-1}. Thus, these discrete exchangers have significantly larger values of ϵ/V than the coaxial tube exchangers, except when R for the discrete exchangers is quite close to 100%. Our first thought, then, is to obtain even higher values of ϵ/V in sintered copper exchangers by using copper powder of smaller diameter than the 44 μm (−325 mesh) size customarily used. The impedance problem at the lowest temperatures is easily overcome because of the high thermal conductivity of the liquids. A small hole through the centre of the sintered powder will reduce the flow impedance considerably but will have little effect on the thermal behaviour,[45] whenever $W_l > 1$ in the radial direction, unless the pore size becomes somewhat smaller than even the He^3 quasiparticle mean free path (~1 μm at 10 mK). The use of smaller copper powder, based on preliminary measurements in our laboratory, decreases ϵ/V slightly below that for 44 μm dia powder, because of a thermal resistance due to phonon–electron [46] and phonon–quasiparticle relaxation effects possibly in the small particle and pore sizes. These additional resistances occur when the phonon mean free path, due to collisions with electrons in the metal or due to collisions with He^3 quasiparticles in the liquid, becomes greater than the particle size or pore size, respectively. These effects need to be considered, sintered copper heat exchanger, energy must be transferred from the electrons to the quasiparticles via the phonons. The phonon mean free path in the liquid has been shown by Baym and Ebner [47] to increase very rapidly as the temperature is decreased. For an He^3 concentration of 5% at 20 mK, the phonon mean free path is 13·5 mm. The mean free path of the dominant phonons in copper at 20 mK, according to equation 2 of Pippard,[48] is 0·74 mm and proportional to $1/T$. The two mean free paths become equal for a temperature of about 0·2 K. However, because of the much higher phonon conductivity in the liquid than in copper, a resistivity due to phonon–He^3 quasiparticle relaxation may only contribute a small part to the total resistance. The phonon mean free path should be considerably less in concentrated He^3, and this then suggests that the optimum particle size to use on the concentrated side would be smaller than on the dilute side. Measurements made here tend to support this idea. The work of Roubeau et al,[46] suggests the phonon–electron interaction is very important for temperatures down to about 50 mK. The same argument is true of the foil exchangers except where the two streams are separated by a single foil [46] so that the phonons need not interact with the electrons. If the thickness of this single foil is made the order of half the dominant phonon wavelength (that is, 0·4 μm at 50 mK in a plastic) then the thermal resistance between the two streams could be reduced to a value below the normal Kapitza resistance value.[49] Such thin unsupported films are now commercially available,[50] but the practical problems encountered in using them could possibly prevent their common usage.

Another approach to increase ϵ/V is to increase σ/V in a continuous exchanger. For the same value of ϵ, a continuous exchanger requires about 1·4 times less surface area than a discrete exchanger whose R = 50%. For R values of 20% and 80%, this factor is 1·2 and 2·1, respectively. If a plastic material is used, a σ/V of only about 160 cm^{-1} will give a continuous exchanger an advantage

over present discrete exchangers for all temperatures. For Cu–Ni, a σ/V of around 600 cm^{-1} would be required to achieve the same ϵ. A sintered powder technique could be used with plastic or Cu–Ni to increase σ/V, but the increase may also be accomplished by decreasing the tube diameters. Several parallel tubes may be required to keep down the flow impedance. Alternatively, closely spaced parallel plates could be used, possibly in an annular configuration using three close fitting coaxial tubes of large diameter. A plastic continuous exchanger with a tube diameter smaller than about 0·25 mm, or a plate spacing of less than 0·06 mm, would then have an ϵ/V value greater than usually found in discrete exchangers. Though this approach has great potential, it may be fraught with practical problems. For one thing, the thermal resistance in the plastic should be small compared with the Kapitza resistance, and this would require the thickness of the plastic separating the two streams to be the order of 0·2 mm or less, depending on the type of plastic.

As one makes the tube diameters (or plate spacing) smaller and increases the number of tubes in parallel (or the plate width), eventually the point is soon reached where the temperature rise due to viscous heating balances the temperature drop due to an increased surface area. The impedance can be reduced again by decreasing the length and increasing the width of the exchanger, but soon the point is reached where axial thermal conduction becomes important. The theoretical maximum in ϵ/V is then found when all three of these conditions (surface area, impedance, and conduction) are optimized simultaneously. In addition, the pressure drop on the dilute side must be kept less than about 7×10^2 N m^{-2} (5 torr) to prevent an increased He^4 circulation. An exact optimization can only be done by solving the full differential equations in (24), although a simple approximate analysis is done here just to show that with a more optimum geometry, ϵ/V can be increased by about an order of magnitude over that for typical co-axial tube exchangers now in use. Thus, such a continuous exchanger would be as good as, or better than, present day discrete exchangers for all temperatures First we require that Y_b in (18) is small compared with Y_l. In fact, it turns out for a practical geometry $Y \simeq Y_d$. This is usually so because the length and width of a parallel plate exchanger will be the same for both the dilute and concentrated phases. Only the plate spacing will be much smaller in the concentrated phase. Thus, for this simple analysis we require $\sigma_c = \sigma_d = \sigma$. For some desired mixer temperature, T_m, the surface area will need to be greater than that shown in Figure 9 or that determined by (25). The increased area needed because of a finite Y is found from Figure 9 or (25) by using the temperature T_m (0) defined as

$$T_m(0) = \frac{T_m}{(1+Y)} \tag{31}$$

We now consider the additional rise in mixer temperature caused by viscous heating in the two streams and balance this out by additional surface area. In this analysis the temperature rise of the mixer due to the viscous heating is chosen to be equally divided between the dilute and concentrated streams. Such a distribution gives about the minimum total heat capacity of the liquids. For the minimum total liquid volume, the dilute side should contribute over 50% of the total viscous heating, but somewhat less than 50% if the moles of He^3 are minimized. For the dilute side, the balance between viscous heating and additional surface area for a fixed liquid volume, V_d, and exchanger length, L, is roughly expressed as

$$\xi_d \frac{\eta_d(T_m) v_3^2 \dot{n}_3}{C_d(T_m)} \left(\frac{\partial Z}{\partial \sigma}\right)_{V_d,L} = -\frac{1}{2}\frac{1}{\dot{n}_3}\left[\frac{dT_m}{d(\sigma/\dot{n}_3)}\right]_{T_m = T_m(0)} \tag{32}$$

The factor ξ_d is determined by solving, for a few examples, the differential equations in (24), including the viscous term but not the thermal conduction term. Corrections for the thermal conduction are calculated by using Y_d. The factor ξ_d is found to be constant to within about 30% and has the value 4×10^{-3}. With the proper values [11,13] for the terms on the left-hand side of (32), this equation becomes

$$\frac{(3{\cdot}5 \times 10^{-13}\ \text{cm}^3\ \text{K}^4\ \text{s mole}^{-1})\dot{n}_3}{T_m^3}\left(\frac{\partial Z}{\partial \sigma}\right)_{V_d,L} = -\frac{1}{2}\frac{1}{\dot{n}_3}\left[\frac{dT_m}{d(\sigma/\dot{n}_3)}\right]_{T_m = T_m(0)} \tag{32a}$$

For a set of parallel plates, the impedance for laminar flow is $Z = 12L/wt^3$, where L, w, and t are the length, width, and spacing of the plates. The term $(\partial Z/\partial\sigma)_{V_d,L}$, using (18) and (19), takes on the form

$$\left(\frac{\partial Z}{\partial \sigma}\right)_{V_d,L} = 24\kappa_d \sigma V_d^2 C_d \dot{n}_3 Y_d \simeq \frac{(9{\cdot}6 \times 10^{-4}\ \text{mole s}^{-1}\ \text{cm}^{-1})\sigma}{V_d^2 \dot{n}_3 Y_d} \tag{33}$$

Equation 32a is solved for V_d with the aid of (25) and (33); and the rest for a set of parallel plates is

$$V_d^2 = (13 \times 10^{-16}\ \text{cm}^2\ \text{K}^4)\frac{\dot{n}_3\,\sigma(\sigma/\dot{n}_3)^{3/2}}{T_m^3 Y_d a} \tag{34}$$

where a is the coefficient in (25) and the surface area σ is that necessary to reach T_m (0). We use (25) and (31) to substitute for σ, which gives the dependence of V_d on Y_d. The minimum V_d is then found to occur when $Y_d = 0{\cdot}25$. The first approximation for σ to use in (34) is just that required in (25) to give a temperature of $T_m/1{\cdot}25$. With V_d and σ known for the parallel plates, the various dimensions are given by $t_d = V_d/\sigma$, $L^2 = V_d L/A \simeq (16 \times 10^{-5}$ moles^{-1} cm^{-1}) V_d/n_3, and $w = V_d/Lt$. The impedance is calculated and the increase in T_m which it causes is just that given by the left-hand side of (32a) with the partial derivative replaced by Z. This temperature rise is subtracted from $T_m/1{\cdot}25$ to give a new value of T_m (0). The value of σ required in (25) to reach such a temperature is the second approximation to use in (34). The process soon converges and it is found that for $T_m \leqslant 40$ mK, the surface area required is approximately

$$\sigma = 2{\cdot}5\,\sigma_0 \tag{35}$$

where σ_0 is the area required to reach T_m when neither conduction nor viscous heating are present. The dilute side volume is then given approximately by

$$V_d = (2{\cdot}3 \times 10^{-7}\ \mathrm{K^2\ cm})\frac{a^2\,\dot{n}_3}{T_m^4} \tag{36}$$

The other plate dimensions are calculated as discussed above. The spacing for the concentrated side is chosen such that the resultant impedance will cause a rise in T_m due to the viscous heating, given by

$$\Delta T_m = \frac{\xi_c\,\gamma\,\eta_c\,\nu_3^2\,\dot{n}_3\,Z}{C_c} \tag{37}$$

equal to that on the dilute side. In (37), ν_3 is now the molar volume of pure He^3 and the terms η_c and C_c are evaluated at the temperature $T_m/\gamma \simeq T_m/0{\cdot}36$. The empirial factor ξ_c was determined in a manner as was ξ_d, and was found to have the approximate value 0·2. The much larger value of ξ_c compared with ξ_d was at first surprising, but is reasonable, since most of the viscous heating occurs near the end of the exchanger where little opportunity exists for this heat to be transferred to the dilute stream. However, for viscous heating in the dilute stream, the resulting temperature rise of the stream through most of the exchanger has little effect on the concentrated stream temperature, T_c, since the heat transferred is roughly proportional to $(T_c^4 - T_d^4)$. This behaviour suggests that all thermal tempering of leads or other heat links be made to the dilute stream only. After substituting the proper values [11,13] in (37), this equation becomes

$$\Delta T_m = \frac{(4 \times 10^{-14}\ \mathrm{K^4\ cm^3\ s\ mole^{-1}})\dot{n}_3\,Z}{T_m^3} \tag{37a}$$

As an example of the optimization procedure for the parallel plate exchanger, suppose we wish to reach $T_m = 10$ mK at a flow rate of $\dot{n}_3 = 2 \times 10^{-5}$ mole s^{-1} with a plastic exchanger. From (35), (36), and (37a), the approximate optimum geometry is such that on the dilute side, $V_d = 0{\cdot}10\ \mathrm{cm^3}$, $t_d = 9{\cdot}0 \times 10^{-4}$ cm, $L = 0{\cdot}90$ cm, and $w = 125$ cm. The pressure drop, given by $\Delta P = \eta_d\,V_3\,\dot{n}_3 Z$, is only about $3 \times 10^2\ \mathrm{N\ m^{-2}}$ (2 torr) and should have little effect on increasing He^4 circulation. For the concentrated side, $V_c = 0{\cdot}050\ \mathrm{cm^3}$ and $t_c = 4{\cdot}4 \times 10^{-4}$ cm. These volumes are about six times less than required with a set of three optimized sintered copper exchangers preceded by a small coaxial tube exchanger. Thus, ϵ/V is also a factor of six higher. The surface to volume ratios for this parallel plate exchanger are $1\,100\ \mathrm{cm^{-1}}$ on the concentrated side, and are over an order of magnitude greater than for a typical co-axial tube configuration.[41] The small values of t on both the dilute and concentrated sides could make such an exchanger difficult to construct in practice. (Different flow rates would change w, but not L or t). Even smaller values of t would occur at higher T_m, so that the optimum design for the parallel plate exchanger would probably only be achieved for $T_m \leqslant 10$ mK. At higher temperatures, one may wish to approach this optimum geometry as close as practically possible. Note that this parallel plate exchanger which has been discussed is a continuous exchanger; thus, it is completely different than a discrete copper foil exchanger.[38] Even higher values of ϵ/V would be possible with many parallel co-axial tubes optimized as was done for the parallel plate exchanger. However, the practical difficulties would be even greater.

Note that the volume given in (36) is simply proportional to $\dot{n}_3$. Since L and t are independent of $\dot{n}_3$, we have $w \propto \dot{n}_3$ and, thus, $Z \propto 1/\dot{n}_3$. The pressure drop is then independent of $\dot{n}_3$. As a result, there is no change in behaviour when scaling the flow rate. Such is the case in discrete exchangers, also. For the behaviour to remain the same we require $\sigma/\dot{n}_3$, w, and ΔP to remain constant. Thus $\sigma \propto \dot{n}_3$, $A \propto \dot{n}_3$, and L = const, keep $\sigma/\dot{n}_3$ and w constant. Since in a discrete heat exchanger, $Z \propto 1/A$, we then have ΔP = const. What this says is simply that only the cross-sectional area of each discrete exchanger should be scaled with flow rate and the length should remain the same to give the same ultimate temperature and same cool-down time. Of course this rule breaks down whenever the ultimate temperature is governed by a residual heat leak. Then higher flow rates would give a lower temperature. Flow rates in actual refrigerators have ranged from just a few μmole s^{-1} to as much as 300 μmole s^{-1}.

Mixing chamber

The thermodynamic behaviour of the mixing chamber is well understood and is discussed in some of the proceeding sections. However, at low-operating temperatures it can be quite difficult to utilize the full refrigeration capability of the mixer because of the ever-present problem of Kapitza resistance. To maintain the temperature of a heat generating source to within 10% of the mixer temperature, requires a copper surface area of about

$$\sigma = \frac{(7 \times 10^2\ \mathrm{cm^2\ K^2\ W^{-1}})\dot{Q}}{T^4} \tag{38}$$

immersed in the dilute He^3 phase. About three times this amount would be required for heat transfer to the concentrated phase because of its higher Kapitza resistance.[13] If the power, $\dot{Q}$, is set equal to the maximum power, $82\,\dot{n}_3\,T^2$ $\mathrm{J\ K^{-2}\ mole^{-1}}$, which can be absorbed by the mixer, then the required surface area is about

$$\sigma = \frac{(6 \times 10^4\ \mathrm{cm^2\ K^2\ s\ mole^{-1}})\,\dot{n}_3}{T^2} \tag{39}$$

For a flow rate of 2×10^{-5} mole s^{-1} and a mixer temperature of 20 mK, this surface area is about $3 \times 10^3\ \mathrm{cm^2}$. Naturally, sintered copper power is generally used inside the mixing chamber to provide this high surface area. The experiment or thermometer is then fastened on the outside of the mixing chamber by a method which has a low thermal resistance, such as a screw contact,[51] indium soldering,[51] or a gold plated collet.[52]

The most reliable and accurate method of measuring the temperature of the liquids inside the mixer is by susceptibility measurements on powdered cerium magnesium nitrate (CMN) in the form of a right circular cylinder, with length equal to the diameter,[13] immersed in the liquid. The measurement of the CMN susceptibility with either mutual inductance or self-inductance coils then requires that the mixer be made of a non-magnetic material of high

electrical resistivity, such as an epoxy.[13] Measurement of the static susceptibility, or magnetization, of the powdered CMN eliminates the resistivity requirement, and allows the mixer to be made of copper. The superconducting quantum interference device (SQUID) makes an extremely sensigive magnetometer [53] for measurement of the static susceptibility, using only a few milligrams of CMN. When a c susceptibility measurements are used, the provision for high surface area inside an epoxy mixer is considerably more complicated, since eddy current heating must be prevented. Mota and Wheatley [54] describe one technique which used bundles of fine copper wire. In our laboratory we have used several narrow strips of 0·11 mm thick copper foil with a 0·13 mm thick layer of sintered copper powder on one surface.[55] Each strip has a copper wire hard soldered in a helium atmosphere to one end of the bare surface, and these wires pass through the wall of the epoxy mixing chamber.

The best position for the powdered CMN in the mixing chamber was at first thought to be at the top, in the pure He^3 phase.[13] The incoming warm He^3 must then be brought in from the bottom to prevent a thermal gradient within the pure He^3 phase. Since the Kapitza resistance between CMN and pure He^3 is anomalously low,[56] it seemed natural to put the CMN there. However, W. C. Black [42] has found that something less than 100 p p m of He^4 in the He^3 can cause the normal Kapitza resistance to reappear. An adsorbed film of He^4 should cover the CMN in the mixing chamber,[57] so there is no longer the advantage of low Kapitza resistance in placing it in the upper phase. In fact, it has been our experience that for mixer temperatures in the range 0·1 K to 0·5 K, this arrangement suffers from very long thermal time constants. This occurs because of the high specific heat per unit volume and low thermal conductivity of the concentrated He^3 in this temperature range. For this reason, it might then be better to place the powdered CMN in the flowing dilute phase, since its thermal conductivity is much higher than concentrated He^3 in this temperature range, and the specific heat per unit volume is less. A second advantage is that the CMN can actually be placed downstream some distance from the mixer so that the mixer itself can be made with copper walls lined with sintered copper powder. Ehnholm and Gylling [58] use such an arrangement. Heat is readily transported from the mixer to the CMN by He^3 mass flow and the time required for the dilute He^3 to travel from the mixer to the CMN powder can be quite short. For $n_3 = 2 \times 10^{-5}$ mole s^{-1} in a tube of 3 mm diameter, the dilute He^3 travels at a speed of about 1 mm s^{-1}. When the CMN is in the flowing dilute phase, one must ensure that the flow impedance between the mixer and a point just past the CMN is sufficiently small to prevent viscous heating; otherwise the CMN will not be indicating the mixer temperature, but in some cases this may not be important. The temperature rise in a flowing He^3 stream at low temperatures is given by [13]

$$\frac{\Delta T}{T} = \zeta \left(\frac{Z}{10^8 \text{ cm}^{-3}} \right) \left(\frac{\dot{n}_3}{10^{-5} \text{ mole s}^{-1}} \right) \left(\frac{20 \text{ mK}}{T} \right)^4 \quad (40)$$

where the coefficient ζ is 0·07 for the concentrated stream and 0·54 for the dilute stream. For a dilute stream temperature of 10 mK and a flow rate of 2×10^{-5} mole s^{-1} through a 3 mm diameter tube, 50 mm long, the temperature rise is 0·4%. Thus, at these temperatures, if the CMN is to accurately measure the mixer temperature, the dilute stream tube will need to be at least 3 mm diameter for this flow rate, about twice as large as is normally used. In addition, a bypass channel will be necessary to carry most of the dilute He^3 around the CMN powder, since the flow impedance through the powder can be sufficiently high at these temperatures to cause significant heating. The flow impedance through various powder sizes has been measured by Betts and Marshall.[45]

Because of the lower Kapitza resistance between copper and dilute He^3 compared with copper and pure He^3, the heat to the mixer should be applied to sintered copper powder in the dilute phase, but not necessarily near the interface. As a matter of fact, the heat can be applied anywhere along the dilute stream between the interface and the entrance to the lowest heat exchanger—the refrigeration rate is always the same and given by (6) or (11). In deriving the thermodynamic behaviour of the mixer it was not necessary to specify where the heat should be applied within the open system in Figure 3. The open system can very well include the inlet and outlet tubes connected to what is normally considered the mixing chamber. The application of heat downstream from the mixing chamber means that the liquid temperature in the mixing chamber will be lower than at the point of application of heat. Suppose one had two types of experiments one with a constant large source of heat for example, a radioactive sample, and the other with negligible heat generation. Then by placing the first downstream from the mixer and the second on the mixer, the two could be carried out simultaneously and would allow the second experiment to reach a lower temperature than it could if both experiments were mounted on the mixing chamber. We now see that one of the beauties of the dilution refrigerator is its ability to pipe refrigeration to any desired point.

Conclusion

The thermodynamics of the dilution refrigerator have been well understood, both qualitatively and quantitatively, for the last few years. For the most part, the few experimental tests of the refrigerator have agreed with the calculated thermodynamic behaviour. As outlined in the text, it now has become possible to predict the behaviour of various types of heat exchangers, provided the heat transfer surface areas and Kapitza resistances are known. This knowledge allows one to build more optimum heat exchangers, and in some cases the same lowest temperature could be reached with liquid volumes reduced as much as an order of magnitude below that now customarily used. Alternatively, with the same liquid volume, much lower temperatures could be achieved.

Many practical improvements in the refrigerator have occurred in the last few years which allow either more efficient operation or easier construction. It has been reported [59] that B. S. Neganov has reached a continuous temperature of 5·5 mK, which is quite close to the practical limit of about 4 mK. Anderson has described [41] a very simple co-axial tube type of dilution refrigerator for reaching about 40 mK. In the next few years, significant practical improvements, particularly in heat exchangers, should occur. Plastic heat exchangers may become common-place, and could permit 5·5 mK to be reached with much smaller heat exchangers. Leggett and Vuorio [60] have suggested that weakly magnetic materials may offer significantly lower Kapitza resistance to He^3 because of the spin coupling between electrons and He^3. Whether this coupling

could still exist in the presence of an adsorbed He^4 film [57] is somewhat doubtful. Certainly, this is a point which needs investigation.

The significant number of dilution refrigerators which have experienced some operating problems is, in most cases, probably a result of various unseen practical errors rather than due to some unknown phenomena. However, the possibility of an abnormal heat leak due to an osmotic pressure induced counterflow of He^3 on the concentrated side has been considered by several people.[61,63] Whenever a connected filament or section of the dilute phase exists in the concentrated He^3 side between two different temperatures, a counterflow of He^3 takes place. This occurs because the osmotic pressure of the He^3 saturated dilute phase is greater at the warm end than at the cold end of the filament or section. At this point, no one seems to know the configuration of the dilute phase and to what extent counterflow heat leak might occur. Certainly, a film of He^4 is adsorbed on the tube walls. Precautions have been made in the past to reduce the effect, if it occurs, by using the smallest possible tubes for the concentrated side without adding a significant amount of viscous heating. The possibility of convective instabilities on the dilute side is also discussed in some detail by Wheatley et al.[63] The poor performance of a refrigerator when the gas is initially condensed on the still side of the pumping line has been reported by Anderson.[41] Others have seen effects of this also. Anderson ascribes such a behaviour to the thicker He^4 film which forms at the higher pressures, in addition to air impurities be ing deposited around the still orifice. Both cause a higher He^4 film flow rate.

The high Kapitza resistance at temperatures encountered in the dilution refrigerator prompted the use of high surface area materials, such as sintered copper. Electron–phonon [62] and phonon–He^3 quasiparticle thermal resistances can become important for these small dimensions, and detailed studies of these resistances would be useful for understanding and improving heat transfer with He^3 or He^3–He^4 solutions at these low temperatures. These additional resistances could have some bearing on the difficulty Wheatley et al [63] have experienced in trying to reach temperatures below 10 mK.

REFERENCES

1. LONDON, H. Proc Int Conf Low Temp Phys, Oxford, 1951, p 157.
2. LAUNDAU, L. D., and POMERANCHUK, I. *Dokl Akad Nauk SSSR* **59**, 669 (1958); POMERANCHUK, I. *Zh Eksperim i Teor Fiz* **19**, 42 (1949).
3. DAS, P., de BRUYN OUBOTER, R., and TACONIS, K. W. in Proc LT9, Columbus, Ohio, 1964, Vol B, p 1253.
4. LONDON, H., CLARKE, G. R., and MENDOZA, E. *Phys Rev* **128**, 1992 (1962).
5. WALTERS, G. K., and FAIRBANK, W. M. *Phys Rev* **103**, 262 (1956).
6. HALL, H. E., FORD, P. J., and THOMPSON, K. *Cryogenics* **6**, 80 (1966).
7. NEGANOV, B., BORIZOV, N., and LIBURG, M. *Zh Eksperim i Teor Fiz* **50**, 1445 (1966) [English transl: *Soviet Phys JETP* **23**, 959 (1966)]; BORIZOV, N. S. KVITKOVA, N. I., LIBURG, M. Yu, NEGANOV, B. S., and TAGIROVA, F. A. Proc LT 10, Moscow, 1966.
8. PESHKOV, V. P. Proc Lt 10, Moscow, 1966; *Zh Eksperim i Teor Fiz* **51**, 1821 (1966) [English transl: *Soviet Phys JETP* **24**, 1227 (1967)].
9. VAROQUAUX, E. 'Polarized targets and ion sources', Proc Int Conf, Saclay, France, 1966, p 169.
10. VILCHES, O. E., and WHEATLEY, J. C. *Phys Lett* **24A**, 440 (1967); ABEL, W. R., and WHEATLEY, J. C. *Phys Lett* **27A**, 599 (1968).
11. RADEBAUGH, R. NBS Technical Note 362, (1967).
12. WHEATLEY, J. C. *Am J Phys* **36**, 181 (1968).
13. WHEATLEY, J. C., VILCHES, O. E., and ABEL, W. R. *Physics* **4**, 1 (1968).
14. NEGANOV, B. S. *Vestn Akad Nauk SSSR*, No 12, 49 (1968).
15. EDWARDS, D. O., BREWER, D. F., SELIGMAN, R., SKERTIC, M , and YAQUB, M. *Phys Rev Lett* **15**, 773 (1965).
16. DE BRUYN OUBOTER, R., TACONIS, K. W., LE PAIR, C., and BEENAKKER, J. J. M. *Physica* **26**, 853 (1960).
17. BREWER, D. F., and KEYSTON, J. R. G. *Phys Lett* **1**, 5 (1962).
18. GRAF, E. H., LEE, D. M., and REPPY, J. D. *Phys Rev Lett* **19**, 417 (1967).
19. IFFT, E. M., EDWARDS, D. O., SARWINSKI, R. E., and SKERTIC, M. M. *Phys Rev Lett* **19**, 831 (1967); EDWARDS, D. O., IFFT, E. M., and SARWINSKI, R. E. *Phys Rev* **177**, 380 (1969).
20. SCHERMER, R. I., PASSEL, L., and RORER, D. C. *Phys Rev* **173**, 277 (1968).
21. ABRAHAM, B. M., BRANDT, O. G., ECKSTEIN, Y., MUNARIAN, J., and BAYM, G. *Phys Rev* **188**, 309 (1969).
22. LANDAU, J., TOUGH, J. T., BRUBAKER, N. R., and EDWARDS, D. O. *Phys Rev Lett* **23**, 283 (1969); *Phys Rev* **2A**, 2472 (1970).
23. BARDEEN, J., BAYM, G., and PINES, D. *Phys Rev* **156**, 207 (1967).
24. ANDERSON, A. C., EDWARDS, D. O., ROACH, W. R., SARWINSKI, R. E., and WHEATLEY, J. C. *Phys Rev Lett* **17**, 367 (1966); ANDERSON, A. C., ROACH, W. R., SARWINSKI, R. E., and WHEATLEY, J. C. *Phys Rev Lett* **16**, 263 (1966).
25. EBNER, C. *Phys Rev* **156**, 222 (1967).
26. SELIGMANN, P., EDWARDS, D. O., SARWINSKI, R. E., and TOUGH, J. T. *Phys Rev* **181**, 415 (1969).
27. WILSON, M. F., and TOUGH, J. T. *Phys Rev* **1A**, 914 (1970).
28. RADEBAUGH, R., and SIEGWARTH, J. D. Proc 1970 Ultralow Temp Symp, Washington, NRL Report 7133, p 63.
29. STONER, E. C. *Phil Mag* **25**, 899 (1938).
30. LONDON, H., PHILLIPS, D., and THOMAS, G. P. Proc Lt 11, St Andrews, Scotland, 1968.
31. GHOZLAN, A., PIEJUS, P., and VAROQUAUX, E. *CR Akad Sci (Paris)* **269B**, 344 (1969).
32. DE LONG, L. E., SYMKO, O. G., and WHEATLEY, J. C. *Rev Sci Instrum* **42**, 147 (1971).
33. See, for example, the papers by WILKES, W. R.; WIEDEMANN, W., PROBST, Chr., and KRAUS, J.; and DAUNT, J. G., and LERNER, E. Proc IIR Commission I Meeting, Tokyo, 1970.
34. BLACK, W. C., HIRSCHKOFF, E. C., MOTA, A. C., and WHEATLEY, J. C. *Rev Sci Instrum* **40**, 846 (1969).

35. CRITCHLOW, P. R., HEMSTREET, R. A., and NEPELL, C. J. *Rev Sci Instrum* **40**, 1381 (1969).
36. TACONIS, K. W., DAS, P., and DE BRUYN OUBOTER, R. 12th Int Congress of Refrigeration, Madrid, Spain, 1967.
37. EDWARDS, D. O. Proc 1970 Ultralow Temp Symp, Washington, NRL Report 7133, p 27.
38. ROUBEAU, P., and VAROQUAUX, E. *Cryogenics* **10**, 255 (1970).
39 SIEGWARTH, J. D., and RADEBAUGH, R. *Rev Sci Instrum* (forthcoming).
40. NEGANOV, B. S. Preprint, Joint Institute for Nuclear Research, Dubna (USSR) (JINR–P13–4014), (1968) [English transl. BNL–TR–234].
41. ANDERSON, A. C. *Rev Sci Instrum* **41**, 1446 (1970); and private phone conversation, (1970).
42. WHEATLEY, J. C. private communication, phone conversation (1970).
43. ANDERSON, A. C., CONNOLLY, J. I., and WHEATLEY, J. C. *Phys Rev* **135**, A910 (1964). The use of a trade name is necessary to make this paper self-contained and does not imply endorsement of that product by the National Bureau of Standards.
44. SYDORIAK, S. G. private communication during laboratory visit (1968).
45. BETTS, D. S., and MARSHALL, R. *Cryogenics* **9**, 460 (1969).
46. ROUBEAU, P., LE FUR, D., and VAROQUAUX, E. J-A. Proc ICEC3, Berlin, 1970, p 315.
47. BAYM, G., and EBNER, C. *Phys Rev* **164**, 235 (1967).
48. PIPPARD, A. B. *J Phys Chem Solids* **3**, 175 (1957).
49. BLAISSE, B. S. Proc IIR Commission I Meeting, Tokyo, 1970, p 79.
50. SPIVAK, M. A. *Rev Sci Instrum* **41**, 1614 (1970).
51. SUOMI, M., ANDERSON, A. C., and HOLMSTROM, B. *Physica* **38**, 67 (1968).
52. BOUGHTON, R. I., BRUBAKER, N. R., and SARWINSKI, R. J. *Rev Sci Instrum* **38**, 1177 (1967).
53. GOODKIND, J. M., and STOLFA, D. L. *Rev Sci Instrum* **41**, 799 (1970); HIRSCHKOFF, E. C., SYMKO, O. G., VANT-HULL, L. L., and WHEATLEY, J. C. *J Low Temp Phys* 2,653 (1970).
54. MOTA, A. C., and WHEATLEY, J. C. *Rev Sci Instrum* **40**, 379 (1969).
55. Kindly furnished to us by E. G. FARRIER of the Union Carbide Corporation, Parma Technical Center, Cleveland.
56. ABEL, W. R., ANDERSON, A. C., BLACK, W. C., and WHEATLEY, J. C. *Phys Rev Lett* **16**, 101 (1966).
57. KEYSTON, J. R. G., and HAHEURTE, J. P. *Phys Lett* **24A**, 132 (1967); BREWER, D. F. *J Low Temp Phys* **3**, 205 (1970).
58. EHNHOLM, G. J., and GYLLING, R. G. *Cryogenics* **11**, 39 (1971).
69. See paper of WHEATLEY, J. C. Proc 1970 Ultralow Temp Symp, Washington, NRL Report 7133, p 99.
60. LEGGETT, A. J., and VUORIO, M. *J Low Temp Phys* **3**, 359 (1970).
61. The authors are grateful for valuable discussions with Profs D. O. EDWARDS and J. C. WHEATLEY pertaining to this possibility.
62. Theoretical calculations of a thermal resistance due to electron–phonon interactions in thin foils has just recently been made by SEIDEN, J. *CR Acad Sci, Paris* **271B**, 5, 1152 (1970); **272B**, 5, (1970).
63. WHEATLEY, J. C., RAPP, R. E., and JOHNSON, R.T. *J Low Temp Phys* **4**, 1 (1971).